Title

Manipulation of Cell-Type Selective Antibody Internalization by a Guide-Effector Bispecific Design

Journal

Molecular Cancer Therapeutics, 18(6)

ISSN

1535-7163

Authors

Lee, Nam-Kyung
Su, Yang
Bidlingmaier, Scott
et al.

Publication Date

2019-06-01

DOI

10.1158/1535-7163.mct-18-1313

Peer reviewed

HHS Public Access

Author manuscript

Mol Cancer Ther. Author manuscript; available in PMC 2020 June 01.

Published in final edited form as:

Mol Cancer Ther. 2019 June ; 18(6): 1092–1103. doi:10.1158/1535-7163.MCT-18-1313.

Manipulation of cell-type selective antibody internalization by a guide-effector bispecific design

Nam-Kyung Lee, **Yang Su**, **Scott Bidlingmaier**, and **Bin Liu**[#]

Department of Anesthesia, UCSF Helen Diller Family Comprehensive Cancer Center, 1001 Potrero Ave., 1305, San Francisco, CA 94143-1305

Abstract

Cell-type specific intracellular payload delivery is desired for antibody-based targeted therapy development. However, tumor-specific internalizing antigens are rare to find, and even rarer for those that are expressed at uniformly high levels. We constructed a bispecific antibody that is composed of a rapidly internalizing antibody binding to a tumor-associated antigen EphA2 and a non-internalizing antibody binding to a highly expressed tumor-associated antigen ALCAM. We found that the overall internalization property of the bispecific is profoundly impacted by the relative surface expression level (antigen density ratio) of EphA2 vs. ALCAM. When the EphA2 to ALCAM ratio is greater than a threshold level (1:5), the amount of the bispecific taken into the tumor cell exceeds what is achieved by either the monoclonal internalizing antibody or a mixture of the two antibodies, showing a bispecific-dependent amplification effect where a small amount of the internalizing antigen EphA2 induces internalization of a larger amount of non-internalizing antigen ALCAM. When the ratio is below the threshold, EphA2 can be rendered non-internalizing by the presence of excess ALCAM on the same cell surface. We constructed a bispecific antibody-drug conjugate (ADC) based on the above bispecific design, and found that the bispecific ADC is more potent than monospecific ADCs in tumor cell killing both *in vitro* and *in vivo*. Thus the internalizing property of a cell surface antigen can be manipulated in either direction by a neighboring antigen, and this phenomenon can be exploited for therapeutic targeting.

Keywords

Antibody internalization; bispecific antibody; guide-to-effector ratio; surface expression threshold; antibody-drug conjugates

Introduction

The high specificity of monoclonal antibody is often exploited for targeted therapy development. Ideally, a potent cytotoxic attached to a cell-type specific antibody can route the cytotoxic to the target cell and preferentially accumulate in the target tissue. Antibody-drug conjugate (ADC) is a class of targeted therapeutic that has shown effectiveness in the

Corresponding author: Bin Liu, Ph.D., Department of Anesthesia, 1001 Potrero Ave., 1305, University of California at San Francisco, San Francisco, CA 94143-1305, Tel: 415 206 6973, bin.liu@ucsf.edu.

Potential conflict of interest: The authors are inventors of intellectual properties related to this work. BL is a founder and shareholder of a biotech company that has licensed intellectual properties related to this work.

clinic (1,2). Internalizing antibody is often desired to achieve efficient intracellular payload delivery and tumor killing (1), although the requirement is not absolute for certain drugs such as MMAE that can diffuse through cell membrane to cause a bystander effect (3).

Although conceptually straightforward, target selection in ADC is hindered by the fact that it is rare to find the so-called tumor specific antigens, and even rarer to find those that bear features desired for therapeutic targeting, i.e., uniformly expressed at high levels by cancer cells, and efficiently internalizing. Several approaches have been developed to improve antibody internalization and ADC efficacy. For example, through the biparatopic design and the consequent crosslinking effect, HER2 antigen has been targeted for improved ADC internalization (4). In another example, a bispecific composed of a moderately internalizing antibody arm (anti-HER2) and an internalization-inducing antibody arm (anti-CD63, anti-PRLR, or anti-APLP2) was constructed and used to improve ADC uptake (5–7). However, despite those efforts, the bispecific ADC only showed limited improvement over the parental monospecific anti-HER2 ADC, suggesting that key parameters regarding this design remain to be delineated.

The key question is if the internalization propensity of a given cell surface antigen can be impacted by its neighboring surface antigens, and if so what are the parameters that govern the conversion of a non-internalizing antigen to an internalizing antigen, and vice versa. We have previously developed a guide-effector bispecific system to achieve cell type specific signaling modulation (8). Key to our design is the guide-to-effector ratio and the threshold of guide antigen expression. We hypothesize that internalization can be manipulated by our guide-effector-based bispecific. We developed a bispecific antibody targeting ephrin receptor A2 (EphA2), a rapidly internalizing antigen, and activated leukocyte cell adhesion molecule (ALCAM), a non- or slowly internalizing antigen, and found that the bispecific becomes internalized when the ratio of EphA2 to ALCAM is greater than ~1:5. We further showed that the bispecific effect is different from that of a simple mixture of the two monoclonal antibodies: the number of bispecific molecules delivered into the tumor cell is greater than that of the antibody mix. Therefore, the guide-effector design can cause an amplification effect, starting with a small number of seed internalizing antigen and propagating the internalizing effect cross the more abundant non-internalizing antigen. Interestingly, when the ratio of EphA2 to ALCAM is below the threshold (1:5), the internalizing EphA2 can be rendered non- or slowly internalizing by ALCAM, demonstrating that the conversion is reciprocal depending on the ratio of the guide to effector antigen. Thus when targeted by a bispecific, internalization of a cell surface antigen can be readily manipulated by its neighboring antigen, resulting in either amplified intracellular uptake or greatly retarded internalization depending on the relative abundance of the two antigens, providing an opportunity for therapeutic exploitation of cell membrane dynamics induced by our guide/effector-based bispecific.

Materials and Methods

Cell lines and plasmids

Human embryonic kidney (HEK) lines HEK293 and HEK293A; prostate cancer cell line DU145 and PC3; and pancreatic cancer cell lines Capan-1, Panc-1 and MIA PaCa2 were

obtained from American Type Culture Collection (ATCC). The L3.6pl line was obtained from Dr. Isaiah Fidler (MD Anderson Cancer Center, Houston, TX) (9). The LNCap-C4–2B was originally obtained from UroCor Inc. and maintained in the laboratory (10). Cells were maintained in DMEM or RPMI1640 supplemented with 10% FBS (Fisher Scientific), 100 μg/ml penicillin/streptomycin (Axenia BioLogix) at 37°C, 5% CO_2. Full-length human EphA2 cDNA cloned into pCMV-Entry (Origene) or pLV202 (Origene) was used for transient or stable expression of EphA2, respectively.

Generation of anti-ALCAM scFv antibodies

A naïve scFv-phagemid display library (11) was used for antibody selection. A recombinant human IgG-like V1–V2 domain of ALCAM fused with human IgG2 Fc (A-V-Fc) was produced from HEK293A cells and utilized as an antigen. A-V-Fc was coated on SPHERO™ polystyrene magnetic particles (Spherotech) at 4°C for overnight. Phage library was depleted with uncoated beads in PBS/2% milk, and unbound phages allowed bind to the A-V-Fc-coated beads. The beads were then washed, eluted, and propagated as described previously (8). Individual phage binders were screened by FACS using the ALCAM-expressing DU145 cell line, and DNA sequence of scFvs was analyzed by IgAT tool (12).

Recombinant antibody production

VH and VL antibody genes were amplified from candidate scFv-phagemid by PCR and sub-cloned into Abvec Ig-γ and -λ expression vectors, respectively (13,14). To produce bispecific IgG-scFvs, the anti-ALCAM 3F1 or a non-binding control C10 was utilized as the IgG backbone, and the internalizing scFv was introduced at C-terminus of the λ light chain constant region (CL) by fusion with a $(Gly_4Ser)_3$ linker (8,15). HEK293A cells were transfected with antibody expression plasmids mixed with polyethylenimine (Sigma Aldrich) in Opti-MEM (Life Technologies) for 24 hours. Transfection medium was changed to Freestyle™ 293 (Gibco) and the cells were further cultured up to 8 days. Secreted antibodies were purified from culture supernatants on protein A agarose (Thermo Scientific) and analyzed on SDS-PAGE gradient gels (4–20%).

Generation of stable HEK293-EphA2 cell line

HEK293 cells were transduced with EpAh2-expresssing lentiviral vector and maintained in regular growth medium containing G418 (Sigma). Stable EphA2-expressing clones were identified by FACS using human anti-EphA2 antibody followed by Alexa Fluor® 647-labeled goat anti-human IgG (Jackson ImmunoResearch). Stable clones were further screened by FACS to obtain those that express varying levels of EphA2.

Cell surface antigen copy number measurement

Cell surface antigen copy number (or antigen density) was measured as described (8,14). Briefly, cells were dissociated by 0.25% trypsin digestion, washed and resuspended in FACS assay buffer (PBS, 1% FBS, pH 7.4), incubated with anti-EphA2 or ALCAM antibodies that were conjugated with Alexa Fluor® 647 by Monoclonal Antibody Labeling Kit (Molecular Probes) to detect EphA2 or ALCAM, respectively, and analyzed by BD Accuri C6 (BD Biosciences). Median Fluorescence Intensity (MFI) was converted into Antibody Binding

Capacity (ABC) using Quantum™ Alexa Fluor® 647 MESF and Quantum™ Simple Cellular® anti-human IgG (Bang's Laboratory) according to manufacturer's recommendations. E/A (EphA2/ALCAM) ratios were calculated by dividing the copy number of EphA2 by that of ALCAM for each cell model studied.

Apparent K_D determination

Dissociated cells (~2×10^5) were incubated with varying concentrations of human IgGs for 16 hours at 4°C. Following three washes with ice-cold PBS, cell-bound IgG was detected by Alexa Fluor® 647-labeled goat anti-human IgG (Jackson ImmunoResearch) and analyzed by FACS (8). Apparent K_D value was calculated by a curve-fitting method using GraphPad Prism software (8,14).

Cell surface antigen depletion

Mono- or bi-specific antibodies (100 nM) were incubated with cells cultured in 24-well plates (~80% confluence) for 24 hours, and EphA2 or ALCAM remaining on cell surface was determined using Alexa Fluor® 647-labeled L1A1 anti-EphA2 human IgG (16) or L50 anti-ALCAM mouse IgG (Fisher Scientific), respectively. Cell surface copy number was calculated using methods described above and normalized against a control group without antibody treatment.

Immunofluorescence confocal microscopy

Antibodies were incubated with cells seeded in 8-well culture chamber slides (Fisher Scientific) for the indicated amount of time. To assess pathway of internalization (macropinocytosis), cells were co-incubated with TexasRed-conjugated 70-kDa neutral dextran (ND70-TR, Life Technologies), a marker for macropinocytosis (16). Post incubation cells were fixed with 4% paraformaldehyde (PFA) and permeabilized with PBS/1% FBS/0.2% Triton-X100. Cell-associated antibodies were stained with Alexa Fluor® 488- or 647-labeled goat anti-human IgG (Jackson ImmunoResearch) for 1 hour at room temperature. Lysosomes were detected by rabbit anti-lysosomal-associated membrane protein 1 (LAMP1) antibody (Cell Signaling) followed by incubation with Alexa Fluor® 647-labeled goat anti-rabbit IgG (Jackson ImmunoResearch). For analysis of antibody localization in tumor spheres, spheres were collected by centrifugation at 500 × g for 5 min, washed, fixed, permeabilized, and immunolabeled using antibodies described above. CyGEL™ (Abcam) was used to immobilize spheres in 8-well chamber slide for microscope analysis. For imaging, cells or spheres were counterstained using Hoechst33342 (Thermo Scientific) and imaged by FluoView® FV10i laser confocal microscope (Olympus) with an Olympus 60× phase contrast water-immersion objective.

Tumor sphere formation

Tumor spheres were generated by culturing suspended tumor cells from monolayer culture in serum free medium (SFM) containing DMEM/F12 (Gibco), 20 ng/ml EGF, 10 ng/ml bFGF, 10 ng/ml IGF and 2% B27 supplement (Gibco) in ultra-low attachment 24-well plate (Corning) at 37°C/5% CO_2. For sphere propagate assay, the first generation spheres were trypsinized and sieved through a 40-μm nylon mesh cell strainer (Fisher Scientific) to obtain

a single cell population. 200 cells per well were resuspended in 500 μl SFM, seeded in ultra-low attachment 24-well plate (Corning) at 37°C/5% CO_2 for 24 hours, and treated with indicated antibodies for 2 weeks. Cells were fed with 100 μl SFM every 3 – 4 days. Each well was sectionally scanned using the BIOREVO digital microscope (BZ-9000; Keyence) and merged to display the whole well image. Spheres > 100 μm in diameter were counted.

Site-specific ADC generation

A cysteine residue was introduced to heavy chain position 116 (T116C) of IgG or bsIgG, and site-specific ADCs were generated as described (17) with modifications. Briefly, antibodies in PBS were reduced by incubating with 10-fold molar excess of Tris(2-carboxyethyl)phosphine hydrochloride (TCEP) (Thermo Scientific) at 37°C for 2 hours, purified by Zeba spin desalting column (Thermo Scientific) and buffer-exchanged in PBS/5 mM EDTA. To re-oxidize inter-chain disulfide bonds, reduced antibodies were incubated with 20-fold molar excess of dehydroascorbic acid (dhAA) (Sigma) at 25°C for 3 hours. After buffer-exchange with PBS/5 mM EDTA, the antibody was incubated at 25°C for 1 hour with 3-fold molar excess of maleimidocaproyl-valine-citrulline-p-aminobenzoyloxycarbonyl monomethyl auristatin F (MC-vc-PAB-MMAF) that was synthesized as previously described (14). The final conjugation product was purified by running twice through the Zeba™ spin desalting column (Fisher Scientific) and analyzed by hydrophobic interaction chromatography (HIC)-HPLC using the infinity 1220 LC System (Agilent). Drug to antibody ratio (DAR) is estimated from area integration using the OpenLab CDS software (Agilent) (14).

ADC cytotoxicity

Cells were seeded at 2×10^3/well in 96-well cell culture plates overnight, and incubated with varying concentrations of ADCs for 96 hours. Cell viability was determined using a Calcein-AM cell viability assay kit (Biotium Inc.) (10).

In vivo xenograft study

All animal studies were approved by the UCSF Animal Care and Use Committee (AN092211) and conducted in adherence to the NIH Guide for the Care and Use of Laboratory Animals. NOD/SCID/IL-2R$\gamma^{-/-}$ (NSG) female mice were engrafted with 1×10^6 Capan-1 cells, randomized into 4 groups at day 5 (n = 6 for each group). Mice were treated intravenously with the vehicle PBS or mono- or bi-specific ADCs at 3 mg/kg every 4 days for a total of 4 injections. Tumor size was measured by a caliper, and tumor volume was calculated using the formula $V = (Width^2 \times Length)/2$. Body weight was monitored during the course of the study.

Results

Identification of a high-affinity ALCAM antibody and generation of the ALCAMxEphA2 bispecific

To identify human antibodies against ALCAM, we performed scFv phage display library selection against N-terminal Ig-like V1–V2 domain of ALCAM (Supplementary Fig. S1A). We identified a panel of binding phage by FACS screening on the $ALCAM^{High}$ DU145

prostate cancer cell line (Supplementary Fig. S1B), and further identified an antibody 3F1 that binds with high affinity as an IgG1 (apparent K_D = 20.6 pM) to DU145 cells (Supplementary Fig. S1C). We studied internalization of the 3F1 IgG on a panel of tumor cell lines by confocal microscopy and found that this antibody is non- or slowly internalizing (Supplementary Fig. S1D).

We constructed a tetravalent bispecific IgG-scFv (bsIgG) composed of the non-internalizing anti-ALCAM 3F1 IgG backbone and an internalizing anti-EphA2 scFv (RYR) fused to the C terminus of the 3F1 light chain (Fig. 1A). The anti-EphA2 scFv (RYR) was identified from our previous study where we used high-content analysis to identify macropinocytosing antibodies (16). For control, a non-binding C10 IgG was used to construct the control C10/RYR bsIgG (binding to EphA2 only). SDS-PAGE analysis showed the expected electrophoresis pattern of monoclonal and bispecific antibodies (Supplementary Fig. S2A). We next studied binding specificity of bsIgGs using the HEK293 cell line that expresses ALCAM, and an engineered HEK293 cell line that stably expresses a high level of EphA2 (HEK293-EphA2#2). As shown in Supplementary Fig. S2B, the anti-ALCAM 3F1 IgG bound to both HEK293 and HEK293-EphA2#2 cells as expected. The 3F1/RYR bsIgG bound at a higher level to HEK293-EphA2#2 ($ALCAM^{high}EphA2^{high}$) compared with HEK293 ($ALCAM^{high}EphA2^{low}$). The control C10/RYR bsIgG that binds to EphA2 only showed specific binding to HEK293-EphA2#2 but not HEK293 cells. Using these two cell line models, internalization activity of the 3F1/RYR bsIgG was studied by confocal microscopy. As shown in Fig. 1B, the 3F1/RYR bsIgG acquired effective internalization capacity in an EphA2-dependent manner - it is internalized by the HEK293-EphA2#2 but not the HEK293 cell line. The control C10/RYR bsIgG is internalized by HEK293-EphA2#2 but not HEK293. The result shows that in our guide-effector bispecific design, the internalizing arm (EphA2, the guide) can impart the non-internalizing arm (ALCAM, the effector) and the bispecific as a whole with internalizing properties.

The non-internalizing antigen can be rendered internalizing by the bispecific in a time and guide to effector ratio-dependent manner

To quantitatively investigate cell surface antigen removal by antibody-induced antigen internalization, quantitative FACS analysis was conducted to measure ALCAM and EphA2 copy numbers on the cell surface (herein referred to as antigen density). As shown in Fig. 1C, the ALCAM level on HEK293-EphA2#2 cells incubated with the bispecific 3F1/RYR was decreased by ~ 90% within the first 4 hours of incubation. There was no significant change of the surface ALCAM level after treatment with monoclonal anti-ALCAM 3F1, the control monoclonal C10, or the control bispecific C10/RYR (Fig. 1C). Efficient ALCAM removal from cell surface by 3F1/RYR was only observed in HEK293-EphA2#2 ($ALCAM^{high}EphA2^{high}$) but not HEK293 ($ALCAM^{high}EphA2^{low}$) (Supplementary Fig. S3A). We further sought to determine whether the antigen removal efficiency is influenced by the guide-to-effector ratio (EphA2/ALCAM). To generate HEK293-based cell models with varying EphA2/ALCAM ratios, EphA2 and/or ALCAM levels were manipulated by three ways: 1) transient transfection of EphA2-expressing plasmid, 2) transient co-transfection of EphA2-expressing plasmid and ALCAM-siRNA, and 3) lentiviral transduction of the EphA2 gene to achieve stable EphA2 expression. These cells showed

varying EphA2/ALCAM ratios and varying patterns of surface antigen removal following the bispecific 3F1/RYR treatment. For example, the monoclonal anti-ALCAM 3F1 IgG or the control C10/RYR bsIgG did not remove ALCAM from the cell surface, whereas the 3F1/RYR bsIgG efficiently removed surface ALCAM (Fig. 1D). By Pearson's correlation coefficient analysis, the effect significantly increases as the EphA2/ALCAM ratio increases (Fig. 1D). With regard to EphA2, the anti-ALCAM 3F1 IgG did not reduce surface EphA2 as expected, but the 3F1/RYR and the control C10/RYR that binds to EphA2 removed EphA2 efficiently from the cell surface (Supplementary Fig. S3B). The ability of the bispecific 3F1/RYR to remove surface ALCAM is affected by the ratio of EphA2 to ALCAM (guide to effector antigen ratio, outlined in Fig. 1E). As summarized in Table 1, when the ratio is < 1:5 (0.2), only a small fraction of ALCAM is removed (20–35%). When the ratio is between 0.9–3.5, 45–65% surface ALCAM is removed. When the ratio is > 3.5, greater than 70% of surface ALCAM is removed.

Internalization and non-internalization are interconvertible properties in a bispecific design

While we have shown that a non-internalizing antigen (ALCAM) can be induced to internalize by the anti-EphA2/ALCAM bispecific when the EphA2 to ALCAM ratio is above a threshold, we studied if the rapidly internalizing EphA2 can be rendered slowly or non-internalizing by the presence of ALCAM at certain EphA2 to ALCAM ratio. Using HEK293 cell line ($ALCAM^{high}EphA2^{low}$) as the model, we found that when the EphA2 to ALCAM ratio is < 0.2, EphA2 internalization was greatly retarded, resulting in a higher fraction of surface bound EphA2 when targeted by the 3F1/RYR bsIgG but not the control C10/RYR (Fig. 1F), suggesting that internalization and non-internalization are interconvertible properties and the relative abundance of internalizing vs. non-internalizing antigen profoundly impacts cell surface antigen turn over when targeted by bispecific antibodies (as outlined in Fig. 1G).

Expanding beyond model cell lines: regulation of internalization dynamics in tumor cell by a guide/effector-based bispecific

We next studied bispecific-induced surface antigen dynamics in a panel of pancreatic cancer cell lines with varying guide to effector ratios. We first determined cell surface antigen density of ALCAM and EphA2 by quantitative FACS (Supplementary Table S1). ALCAM is highly expressed by those cells, and the guide to effector (EphA2 to ALCAM) ratio for L3.6pl, Capan-1, and Panc-1 was estimated to be 0.31, 0.23, and 0.08, respectively. We next performed two sets of experiments to determine (1) how the non-internalizing ALCAM is converted into an internalizing antigen by the bispecific with an EphA2 to ALCAM ratio above the threshold (> 0.2); and (2) how the rapidly internalizing EphA2 is rendered slowly internalizing by the bispecific with an EphA2 to ALCAM ratio below the threshold (< 0.2). The internalization dynamics of EphA2 and ALCAM were studied by measuring surface antigen level by FACS following antibody treatment. With regard to ALCAM, the bispecific 3F1/RYR was effective in removing about 60% cell surface ALCAM in both L3.6pl and Capan-1 cells where the guide to effector ratios are > 0.2, but ineffective in Panc-1 cells where the ratio is 0.08, suggesting a cell type selectivity based on the guide to effector ratio (Fig. 2A). The non-internalizing monoclonal anti-ALCAM antibody 3F1 did not remove any ALCAM antigen from the cell surface. The control C10/RYR or an antibody mixture of 3F1

and C10/RYR removed about 85% of surface EphA2 (Supplementary Fig. S3C) but failed to remove ALCAM (Fig. 2A), suggesting that ALCAM removal is a bispecific-dependent phenomenon not achievable by oligoclonal antibody mix. The above bispecific effect on antigen internalization was also studied by confocal microscopy. As shown in Fig. 2B, in L3.6pl cells where the EphA2/ALCAM ratio is > 0.2 (~ 0.31), the anti-ALCAM 3F1 was mostly detected on the cell surface, while the bispecific 3F1/RYR was detected mainly in the cytoplasm with some staining of the cell membrane. The control C10/RYR that binds to EphA2 was detected mainly in the cytoplasm, consistent with its ability to induce rapid EphA2 internalization. In contrast, for the Panc-1 cell line that has a EphA2/ALCAM ratio < 0.2 (~ 0.08), the bispecific 3F1/RYR was detected mainly on the cell surface (Fig. 2B), again suggesting that internalization of the bispecific depends on the EphA2/ALCAM ratio. Those data confirm that in our guide-effector bispecific design, the ability of the bispecific to convert a non-internalizing to internalizing effector antigen depends on the guide to effector ratio.

To assess pathway of internalization and trafficking to the lysosome, we performed confocal microscopy studies using L3.6pl cells. As shown in Fig. 2C, the bispecific 3F1/RYR was colocalized with the macropinocytosis marker, 70 kDa Neutral Dextran (ND70), suggesting the mode of internalization is macropinocytosis. Post internalization, 3F1/RYR and the control C10/RYR were colocalized with the lysosomal marker lysosomal-associated membrane protein 1 (LAMP1) (Fig. 2D), suggesting that the anti-EphA2 antibody-guided bispecific traffics to the lysosome.

To investigate the other direction of the interconversion between internalization and non-internalization, i.e., conversion of a rapidly internalizing antibody into a slowly or non-internalizing antibody, we studied surface removal of EphA2 by the bispecific in the presence of the neighboring non-internalizing antigen ALCAM. As shown in Fig. 2E, on Panc-1 cell where the EphA2 to ALCAM ratio is < 0.2 (~ 0.08), EphA2 remains mainly on the cell surface when targeted by the bispecific 3F1/RYR. The control C10/RYR removes EphA2 from the cell surface. The C10/RYR plus 3F1 mixture does not retard EphA2 internalization, suggesting that the phenomenon is dependent on the bispecific. A time course internalization study shows that the 3F1/RYR greatly retarded EphA2 internalization kinetics, whereas the control C10/RYR induced rapid EphA2 internalization (Fig. 2F). These studies demonstrate that EphA2 internalization can be significantly retarded by the bispecific when ALCAM is present on the same cell with amounts exceeding the threshold level of EphA2/ALCAM ratio.

The bispecific 3F1/RYR inhibits pancreatic tumor-sphere formation

To assess functional consequences of surface antigen removal, we studied effects of the anti-EphA2-guided bsIgG (3F1/RYR) on survival and expansion of pancreatic tumor spheres. Previous studies have shown that cancer cells overexpressing ALCAM aggressively form tumor-spheres, suggesting that ALCAM plays a role in tumor clonogenicity (18–20). We therefore studied whether ALCAM removal by our ALCAMxEphA2 bsIgG can inhibit pancreatic tumor sphere formation. We first assessed antigen expression in L3.6pl tumor spheres and found that ALCAM was significantly upregulated on the surface of sphere-

forming tumor cells (Fig. 3A). There was no difference of EphA2 surface level between L3.6pl cells in monolayer vs. sphere states (Fig. 3A). Following incubation of L3.6pl tumor spheres with antibodies for 2 weeks, the bispecific 3F1/RYR reduced ALCAM surface density by 70%, whereas the anti-ALCAM mAb 3F1 or the control C10/RYR that binds to EphA2 only showed no effect on ALCAM surface level (Fig. 3B). We next performed confocal microscopy study to confirm antibody internalization. As shown in Fig. 3C, 3F1/RYR was effectively internalized in L3.6pl sphere forming cells. In contrast, the monoclonal anti-ALCAM antibody 3F1 showed mainly surface staining (Fig. 3C). The control bispecific C10/RYR was internalized, consistent with its monospecific binding to EphA2 (Fig. 3C). Interestingly, based on the fluorescence signal intensity per cell, a greater amount of the 3F1/RYR was taken up by tumor sphere-forming cells compared with the control bispecific C10/RYR (Fig. 3C, *right panel*), suggesting an amplification effect unique to the bispecific. With regard to functional effect on tumor clonogenic activity, we found that L3.6pl sphere number (Fig. 3D) and size (Fig. 3E) was significantly decreased by treatment with 3F1/RYR but not 3F1 or C10/RYR, consistent with previous studies of the role of ALCAM in tumor sphere formation and growth. Thus the bispecific antibody with one arm binding to the internalizing antigen EphA2 can effectively removed the non-internalizing antigen ALCAM from tumor cell surface, resulting in inhibition of pancreatic tumor sphere growth.

Potent and cell-type selective *in vitro* tumor cell killing by bispecific ADC

To explore therapeutic potential of the bispecific-induced amplification of intracellular uptake, we generated monospecific and bispecific ADCs by site-specific conjugation of MC-VC-pab-MMAF (Supplementary Fig. S4), analyzed conjugation products by HIC-HPLC and determined the drug-to-antibody ratio (~ 1.9) (14,17,21). ADCs were tested on a panel of cancer cell lines that display different levels of cell surface EphA2 and ALCAM, and EphA2 to ALCAM ratios (Supplementary Table S1). The 3F1/RYR ADC showed potent cytotoxicity with EC50 of 23 pM on L3.6pl and 22 pM on Capan-1 cells (Fig. 4A and 4B, and Supplementary Table S2). These two cell lines have EphA2 to ALCAM ratios above the threshold (0.2, Supplementary Table S1), resulting in more efficient internalization. In contrast, both 3F1 and C10/RYR ADCs showed lower potency. EC50 values of 3F1 and C10/RYR ADCs on L3.6pl are 2.37 nM and 0.35 nM respectively, and on Capan-1 are 0.87 nM and 0.18 nM, respectively (Fig. 4A and 4B). Most importantly, the bispecific ADC is more potent than the mix of monoclonal ADCs (C10/RYR ADC + 3F1 ADC, Fig. 4A and 4B), suggesting again that this enhanced potency is unique to the bispecific. We also studied cytotoxicity of ADCs on Panc-1 cells with a low guide to effector (EphA2 to ALCAM) ratio and MIA PaCa2 cells without the effector antigen (ALCAM) expression. On Panc-1 cells with a low EphA2/ALCAM ratio (0.08), the bispecific 3F1/RYR ADC showed reduced potency (EC50 = 0.46 nM) but is still more potent than 3F1 (EC50 = 9.3 nM) and C10/RYR ADCs (EC50 > 100 nM) (Fig. 4C and Supplementary Table S2). Again, the cytotoxic potency of 3F1/RYR ADC was higher than a mixture of the 3F1 and C10/RYR ADCs (EC50 = 0.46 nM vs. 7.14 nM for the mix) (Supplementary Table S2). On the ALCAM-negative MIA PaCa2 cell line, the 3F1 ADC showed little cytotoxicity as expected (Fig. 4D). 3F1/RYR and C10/RYR ADCs showed similarly low cytotoxicity due to the lack of expression of ALCAM and low expression level of EphA2 (Fig. 4D). To further evaluate cell

type selectivity, we studied LNCaP-C4–2B and HEK293 cell lines that express very low levels of EphA2. On LNCaP-C4–2B, as shown in Fig. 4E, the bispecific 3F1/RYR ADC did not show enhanced cytotoxicity vs. the monoclonal 3F1 ADC (EC50 = 1.25 nM vs. 1.64 nM, Supplementary Table S2), due to the lack of the guide antigen EphA2 expression, showing a guide antigen-dependent cell type selectivity. Similar results were obtained from studies using HEK293 cells that lack the guide antigen expression (Supplementary Fig. S5). Taken together, those data show that the bispecific ADC is more potent than mono-specific ADCs or their mixture, and exhibits a cell-type selective potency enhancement depending on the guide to effector antigen ratio.

In vivo anti-tumor efficacy of the ALCAMxEphA2 bispecific ADC

We next studied *in vivo* efficacy of the bispecific 3F1/RYR ADC along with control ADCs on pancreatic cancer xenografts. Capan-1 cells were implanted subcutaneously into NSG mice. When the tumor reached an average volume of 110 mm^3, 3F1/RYR, 3F1, or C10/RYR ADCs were injected at 3 mg/kg every four days for a total of four times. Tumor status was monitored by caliper measurement. Overt toxicity was monitored by body weight loss. As shown in Fig. 5A, the bispecific 3F1/RYR ADC significantly inhibited tumor growth, while the monoclonal 3F1 ADC or the control bispecific C10/RYR ADC had only a moderate effect on tumor size reduction. There was no significant change of body weights during the course of the study for any of the ADCs studied (Fig. 5B). These data demonstrate that in our guide-effector bispecific design, the rapidly internalizing anti-guide (EphA2) scFv can induce internalization of the otherwise non-internalizing effector antigen (ALCAM), resulting in greater amount of bispecific ADCs taken into the tumor cells compared to monospecific ADCs, thus showing enhanced anti-tumor efficacy *in vivo*.

Discussion

In this study we adopted the guide-effector bispecific antibody design that we developed previously for cell-type specific signaling modulation (8), and achieved cell-type specific modulation of internalization. We show that when the guide to effector ratio crosses over a threshold (in our EphA2/ALCAM example, 1:5), a non-internalizing antigen (ALCAM) can be rendered internalizing by the bispecific. When the guide to effector ratio falls below the threshold, an internalizing antigen (EphA2) can be rendered non- or slowly internalizing by the bispecific. Thus in the context of bispecific targeting, the internalization behavior of a cell surface antigen is significantly impacted by its neighboring antigens, and can be readily manipulated in either direction through bispecific-based targeting of appropriately selected guide/effector pairs.

Our study has relevance to therapeutic development. In the direction of converting a non-internalizing into an internalizing antigen, our study has direct relevance to ADC development. ADC is a class of anti-cancer agents that utilize the specificity of the antibody to deliver cytotoxic drug to tumor cells. Although appealing in concept, clinical development of this class of anti-cancer agents has encountered various challenges. So far, there are only 4 ADCs that are approved by the FDA for clinical use. Early problems such as drug and linker stability have been addressed but other issues remain (1). Although very potent drugs

such as DNA chelators have been used for ADC generation, those drugs cause accumulative toxicity, restricting the therapeutic window (22). Microtubule inhibitors such as auristatin derivatives are less potent compared to DNA chelators and their toxicity is not accumulative except for peripheral nerve damage. Because of the reduced potency of auristatin and the limited amount of drug delivered into tumor cell, the therapeutic window remains narrow (1). Increasing DAR can result in more drug molecules delivered to a tumor cell *in vitro*, but *in vivo* ADCs with high DARs are rapidly cleared from the circulation, thus reducing efficacy and increasing toxicity. Site-specific conjugation achieves near uniform DAR (n=2), improves PK but the total number of drug molecules delivered into a tumor cell remains limited (21,23). In principle, ways to improve the therapeutic window of ADC include: (1) Increase cell surface target density; and (2) Improve target internalization. Both should result in a higher number of ADCs delivered intracellularly into the tumor cell. We have previously explored macropinocytosing antibodies for ADC construction to improve internalization (16,24). In this report, we describe our approach to increase target density through a guide-effector bispecific design.

We used a rapidly internalizing macropinocytosing anti-EphA2 (the guide) antibody and a non/slowly internalizing anti-ALCAM (the effector) antibody as a model system to study the bispecific effect. We found that when the antigen density ratio of EphA2/ALCAM is greater than a threshold (1:5 in our experimental system), a bispecific anti-ALCAMxEphA2 antibody can induce internalization of both EphA2 and ALCAM. In other words, the bispecific can turn a non-internalizing antigen (ALCAM) to an internalizing antigen. We found that the bispecific ADC is more potent than either of the monospecific ADCs and furthermore the mixture of these ADCs in *in vitro* cytotoxicity assays, consistent with increased amount of internalized ADC delivered by the bispecific. Thus there is an amplification effect that is unique to the bispecific but not the monospecific antibodies or their mix, where a small number of internalizing antigen (the guide, EphA2), upon targeted by the bispecific, can induce the internalization of a large number of non-internalizing antigen (the effector, ALCAM), resulting in greater amount of ADC and drug molecule delivered to the tumor cell compared to monoclonal ADCs and their mixture.

In addition to enhanced potency through amplified internalization, our study has implication for expanding the range and type of cell surface targets for ADC. A key challenge for current ADC is how to deliver payload specifically and in high amount to target cells. In a monoclonal antibody setting, the target antigen needs to be expressed both specifically and at a uniformly high level on the tumor surface. In practice, however, antigen with both absolute specificity and uniformly high level of expression is rare to find. As such, lineage markers, which are expressed by the tissue from which the tumor is derived, have often been used for tumor targeting (1). There are two limitations for those lineage markers: (1) they tend to show decreased or heterogeneous expression in late-stage cancers as they are not functionally required for tumor survival. For example, PSMA expression in late stage prostate cancer is heterogeneous and is downregulated in androgen signaling inhibitor-resistant small cell type (10). (2) they are often expressed in more than one normal tissue type. For example, while mesothelin is expressed by a number of tumors such as mesothelioma, ovarian cancer, and pancreatic cancer, it is also expressed by the normal mesothelium (25). PSMA is expressed by prostate tumor but also by a number of normal

tissues (26,27). Likewise, CD19 is expressed by normal tissues other than B cells (28). It seems that by the monoclonal antibody approach, the target selection is rather restricted or sub-optimal. In the context of ADC, efforts have been directed to increase potency of the payload but the therapeutic window remains narrow as discussed above. An alternative approach is to identify targets that expand the difference between payloads delivered to tumor vs. normal cells. Our work is particularly relevant to this approach as our guide-effector bispecific design allows a large number of non-internalizing tumor-associated antigens to become internalized and thus contributing to increased intracellular delivery of ADC. The amplification effect is unique to tumor cells due to co-expression of both the guide and effector antigens.

We have previously described the guide-effector bispecific design for cell-type specific signaling pathway modulation (8). This study expands the applicability of the bispecific approach to antigen internalization and ADC. The essence of guide-effector bispecific system is that the behavior of a given antigen (effector) can be shaped by the neighboring antigen (guide) when the ratio of guide to effector exceeds a threshold level. In the Wnt signaling study, when the guide/effector ratio exceeds 5–10:1, there is a thousand-fold increase in potency of the bispecific over the monoclonal antibody and the enhancement is cell-type specific. In this study, we showed that when the guide/effector ratio exceeds 1:5, a small number of the guide antigen (internalizing) can convert a large number of effector antigen (non-internalizing) to internalizing antigen. In both of our studies, the guide to effector ratio (or more precisely, the occupied guide to effector ratio) has the most significant impact, although other factors such as antibody affinity, epitope geometry and membrane microdomain all could affect the outcome depending on the exact antibody and guide/effector pairs chosen.

Interestingly, although our study is focused on ADC and conversion of a non-internalizing antibody into an internalizing antibody, we showed that the reverse is true: when the ratio of internalizing to non-internalizing antigen is below the threshold level (in our system 1:5), the internalizing antigen EphA2 is rendered slowly internalizing by the presence of the non-internalizing ALCAM. This could be useful for applications where it is desirable to have antigen remain on the cell surface to prevent degradation, and to prolong signaling functions.

There are a few recent reports of bispecific ADC with the internalizing arm binding to either a lysosomal protein or an antigen that rapidly traffics to the lysosome (5–7). In most cases, the observation is empirical and the bispecific effect is rather moderate, suggesting that key parameters affecting bispecific-induced internalization have not been fully delineated. For example, it is unclear if lysosomal antigen is required for this phenomenon. It is also unclear why the bispecific works on some cells but not the other. Our study shows that a key variable in the bispecific design is the ratio of the guide to effector antigen, and there is no special feature beyond internalization that is required for the internalizing arm. The guide antigen (the internalizing arm) needs not to be a lysosomal protein to induce internalization and lysosomal trafficking. For example, in this study we exploited macropinocytosis and selected the macropinocytosing antibody against the cell surface antigen EphA2 as the guide to route the bispecific to the lysosomal compartment.

In summary, we show that in the context of bispecific targeting, internalization is no longer an intrinsic property of a given antigen. Instead, antigen internalization is heavily influenced by its neighboring antigens and can be readily manipulated in either direction in a cell-type specific manner using properly selected guide/effector pairs. This bispecific-induced plasticity of cell surface dynamics can be exploited for therapeutic development.

Supplementary Material

Refer to Web version on PubMed Central for supplementary material.

Acknowledgments

We thank Dr. Byron C. Hann for advice, Donghui Wang, Paul Phojanakong, Fernando Salangsang and Julia Malato at the UCSF Preclinical Therapeutic Core for performing animal studies. This research was supported by the National Institutes of Health (R01 CA118919, CA129491, and CA171315 to BL), and a fellowship grant to NKL from the Basic Science Research Program through the National Research Foundation of Korea (NRF) funded by the Ministry of Education, Science and Technology (2013R1A6A3A03060495).

Reference:

1. de Goeij BE, Lambert JM. New developments for antibody-drug conjugate-based therapeutic approaches. Curr Opin Immunol 2016;40:14–23 doi 10.1016/j.coi.2016.02.008. [PubMed: 26963132]
2. Polakis P Antibody Drug Conjugates for Cancer Therapy. Pharmacol Rev 2016;68(1):3–19 doi 10.1124/pr.114.009373. [PubMed: 26589413]
3. Gebleux R, Stringhini M, Casanova R, Soltermann A, Neri D. Non-internalizing antibody-drug conjugates display potent anti-cancer activity upon proteolytic release of monomethyl auristatin E in the subendothelial extracellular matrix. Int J Cancer 2017;140(7):1670–9 doi 10.1002/ijc.30569. [PubMed: 27943268]
4. Li JY, Perry SR, Muniz-Medina V, Wang X, Wetzel LK, Rebelatto MC, et al. A Biparatopic HER2-Targeting Antibody-Drug Conjugate Induces Tumor Regression in Primary Models Refractory to or Ineligible for HER2-Targeted Therapy. Cancer Cell 2016;29(1):117–29 doi 10.1016/j.ccell.2015.12.008. [PubMed: 26766593]
5. de Goeij BE, Vink T, Ten Napel H, Breij EC, Satijn D, Wubbolts R, et al. Efficient Payload Delivery by a Bispecific Antibody-Drug Conjugate Targeting HER2 and CD63. Mol Cancer Ther 2016;15(11):2688–97 doi 10.1158/1535-7163.MCT-16-0364. [PubMed: 27559142]
6. Andreev J, Thambi N, Perez Bay AE, Delfino F, Martin J, Kelly MP, et al. Bispecific Antibodies and Antibody-Drug Conjugates (ADCs) Bridging HER2 and Prolactin Receptor Improve Efficacy of HER2 ADCs. Mol Cancer Ther 2017;16(4):681–93 doi 10.1158/1535-7163.MCT-16-0658. [PubMed: 28108597]
7. DeVay RM, Delaria K, Zhu G, Holz C, Foletti D, Sutton J, et al. Improved Lysosomal Trafficking Can Modulate the Potency of Antibody Drug Conjugates. Bioconjug Chem 2017;28(4):1102–14 doi 10.1021/acs.bioconjchem.7b00013. [PubMed: 28151644]
8. Lee NK, Zhang Y, Su Y, Bidlingmaier S, Sherbenou DW, Ha KD, et al. Cell-type specific potent Wnt signaling blockade by bispecific antibody. Sci Rep 2018;8(1):766 doi 10.1038/s41598-017-17539-z. [PubMed: 29335534]
9. Bruns CJ, Harbison MT, Kuniyasu H, Eue I, Fidler IJ. In vivo selection and characterization of metastatic variants from human pancreatic adenocarcinoma by using orthotopic implantation in nude mice. Neoplasia 1999;1(1):50–62. [PubMed: 10935470]
10. Su Y, Liu Y, Behrens CR, Bidlingmaier S, Lee NK, Aggarwal R, et al. Targeting CD46 for both adenocarcinoma and neuroendocrine prostate cancer. JCI Insight 2018;3(17):pii: 121497 doi 10.1172/jci.insight.121497. [PubMed: 30185663]

11. Lee NK, Bidlingmaier S, Su Y, Liu B. Modular Construction of Large Non-Immune Human Antibody Phage-Display Libraries from Variable Heavy and Light Chain Gene Cassettes. Methods Mol Biol 2018;1701:61–82 doi 10.1007/978-1-4939-7447-4_4. [PubMed: 29116500]
12. Rogosch T, Kerzel S, Hoi KH, Zhang Z, Maier RF, Ippolito GC, et al. Immunoglobulin analysis tool: a novel tool for the analysis of human and mouse heavy and light chain transcripts. Front Immunol 2012;3:176 doi 10.3389/fimmu.2012.00176. [PubMed: 22754554]
13. Smith K, Garman L, Wrammert J, Zheng NY, Capra JD, Ahmed R, et al. Rapid generation of fully human monoclonal antibodies specific to a vaccinating antigen. Nat Protoc 2009;4(3):372–84 doi 10.1038/nprot.2009.3. [PubMed: 19247287]
14. Sherbenou DW, Aftab BT, Su Y, Behrens CR, Wiita A, Logan AC, et al. Antibody-drug conjugate targeting CD46 eliminates multiple myeloma cells. J Clin Invest 2016;126(12):4640–53 doi 10.1172/JCI85856. [PubMed: 27841764]
15. Orcutt KD, Ackerman ME, Cieslewicz M, Quiroz E, Slusarczyk AL, Frangioni JV, et al. A modular IgG-scFv bispecific antibody topology. Protein Eng Des Sel 2010;23(4):221–8 doi 10.1093/protein/gzp077. [PubMed: 20019028]
16. Ha KD, Bidlingmaier SM, Zhang Y, Su Y, Liu B. High-content analysis of antibody phage-display library selection outputs identifies tumor selective macropinocytosis-dependent rapidly internalizing antibodies. Mol Cell Proteomics 2014;13(12):3320–31 doi 10.1074/mcp.M114.039768. [PubMed: 25149096]
17. Junutula JR, Raab H, Clark S, Bhakta S, Leipold DD, Weir S, et al. Site-specific conjugation of a cytotoxic drug to an antibody improves the therapeutic index. Nat Biotechnol 2008;26(8):925–32 doi 10.1038/nbt.1480. [PubMed: 18641636]
18. Jiao J, Hindoyan A, Wang S, Tran LM, Goldstein AS, Lawson D, et al. Identification of CD166 as a surface marker for enriching prostate stem/progenitor and cancer initiating cells. PLoS One 2012;7(8):e42564 doi 10.1371/journal.pone.0042564. [PubMed: 22880034]
19. Yan M, Yang X, Wang L, Clark D, Zuo H, Ye D, et al. Plasma membrane proteomics of tumor spheres identify CD166 as a novel marker for cancer stem-like cells in head and neck squamous cell carcinoma. Mol Cell Proteomics 2013;12(11):3271–84 doi 10.1074/mcp.M112.025460. [PubMed: 23903875]
20. Moon BS, Jeong WJ, Park J, Kim TI, Min do S, Choi KY. Role of oncogenic K-Ras in cancer stem cell activation by aberrant Wnt/beta-catenin signaling. J Natl Cancer Inst 2014;106(2):djt373 doi 10.1093/jnci/djt373. [PubMed: 24491301]
21. Behrens CR, Liu B. Methods for site-specific drug conjugation to antibodies. MAbs 2014;6(1):46–53 doi 10.4161/mabs.26632. [PubMed: 24135651]
22. Fu Y, Ho M. DNA damaging agent-based antibody-drug conjugates for cancer therapy. Antib Ther 2018;1(2):33–43 doi 10.1093/abt/tby007. [PubMed: 30294716]
23. Panowski S, Bhakta S, Raab H, Polakis P, Junutula JR. Site-specific antibody drug conjugates for cancer therapy. MAbs 2014;6(1):34–45 doi 10.4161/mabs.27022. [PubMed: 24423619]
24. Ha KD, Bidlingmaier SM, Su Y, Lee NK, Liu B. Identification of Novel Macropinocytosing Human Antibodies by Phage Display and High-Content Analysis. Methods Enzymol 2017;585:91–110 doi 10.1016/bs.mie.2016.10.004. [PubMed: 28109445]
25. Chang K, Pastan I. Molecular cloning of mesothelin, a differentiation antigen present on mesothelium, mesotheliomas, and ovarian cancers. Proc Natl Acad Sci U S A 1996;93(1):136–40. [PubMed: 8552591]
26. Silver DA, Pellicer I, Fair WR, Heston WD, Cordon-Cardo C. Prostate-specific membrane antigen expression in normal and malignant human tissues. Clin Cancer Res 1997;3(1):81–5. [PubMed: 9815541]
27. Kinoshita Y, Kuratsukuri K, Landas S, Imaida K, Rovito PM Jr., Wang CY, et al. Expression of prostate-specific membrane antigen in normal and malignant human tissues. World J Surg 2006;30(4):628–36 doi 10.1007/s00268-005-0544-5. [PubMed: 16555021]
28. Wang K, Wei G, Liu D. CD19: a biomarker for B cell development, lymphoma diagnosis and therapy. Exp Hematol Oncol 2012;1(1):36 doi 10.1186/2162-3619-1-36. [PubMed: 23210908]

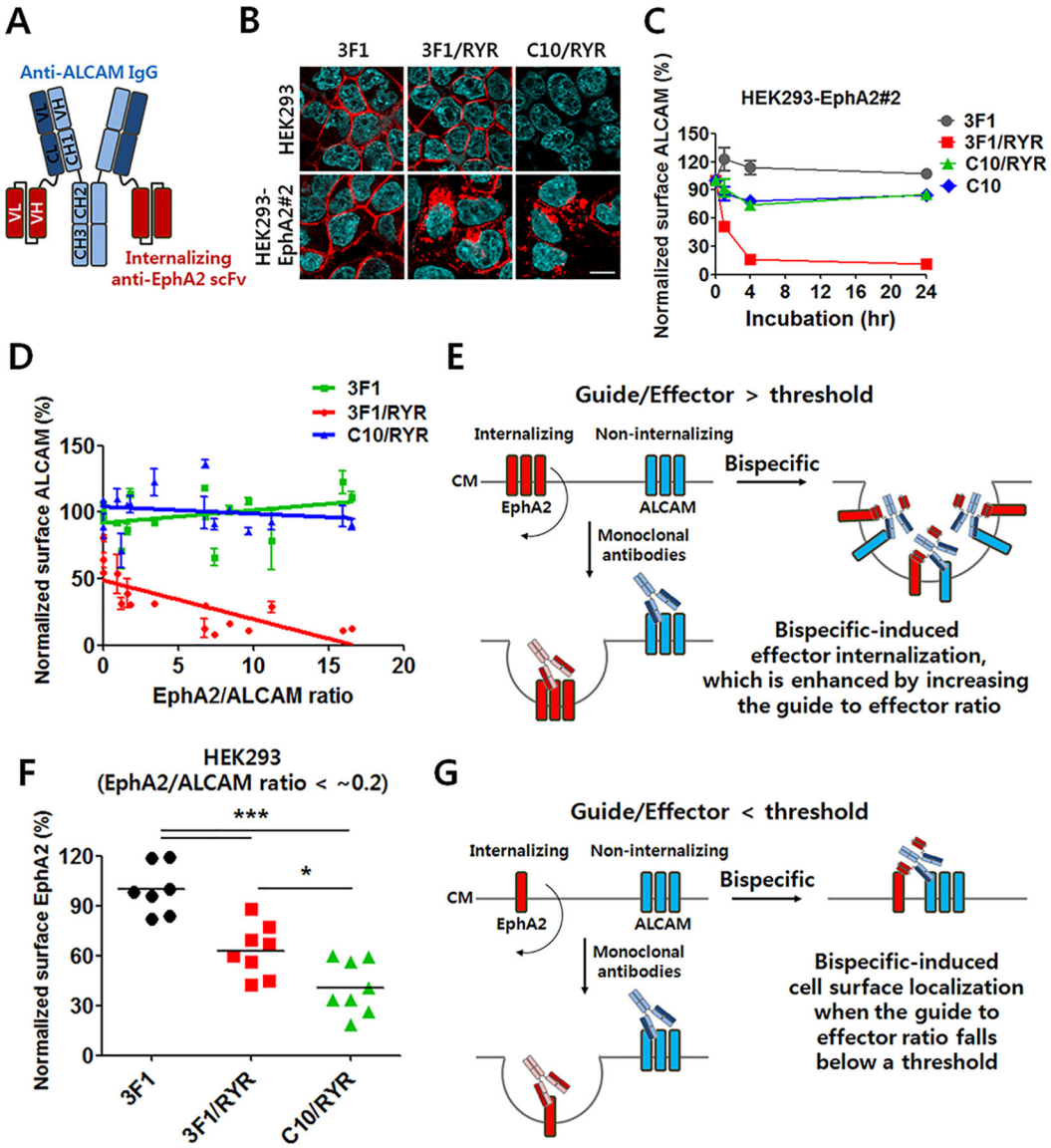

Fig. 1. A bispecific based on the guide-effector design can profoundly impact internalization dynamics of cell surface antigen.

A) Illustration of the tetravalent ALCAMxEphA2 bsIgG. The IgG backbone is based on the non-internalizing anti-ALCAM antibody 3F1. The internalizing anti-EphA2 scFv is fused to the end of light chain C-terminus. B) Confocal microscopy study of antibody internalization. HEK293 or HEK293-EphA2#2 cells were incubated with indicated IgG or bsIgG (100 nM) at 37 °C for 2 hours. Antibodies (*red*) were detected using Alexa® 647-labeled anti-human IgG secondary antibody, and cell images were analyzed using a digital laser confocal microscope. Scale bar: 20 μm. C) Kinetics of ALCAM cell surface removal by the bispecific. HEK293-EphA2#2 cells were incubated with indicated IgG or bsIgG for 1, 4, and 24 hours and surface ALCAM levels determined by FACS. The non-internalizing ALCAM is removed from cell surface by the bispecific (3F1/RYR) but not monoclonal antibodies. D) Correlation between surface antigen (ALCAM) removal efficiency and EphA2/ALCAM (E/A) expression ratio. HEK293 cell models with varying EphA2/ALCAM ratios were

incubated with 3F1, 3F1/RYR, and C10/RYR (all at 100 nM), and antigens remaining on the cell surface were determined by anti-ALCAM antibodies that bind to a different epitope than 3F1. Pearson's correlation coefficient (r) was calculated (0.3266, −0.7550, and −0.1896 for 3F1, 3F1/RYR, and C10/RYR, respectively) and trend-lines were depicted according to linear regression analysis. Data represent mean ± SD (duplicate). E) Illustration depicting bispecific-induced ALCAM internalization when the guide to effector ratio > threshold. CM: cell membrane. F) Significant retardation of EphA2 internalization by the bispecific 3F1/RYR when guide to effector ratio falls below a threshold level. HEK293 cells that possess a low EphA2/ALCAM ratio (< 0.2) were incubated with indicated antibodies (100 nM), and surface EphA2 levels were measured by FACS. P values were determined using two-tailed Student's t-test. *P<0.05, and ***P<0.001. G) Illustration of the phenomenon shown in panel F where EphA2 internalization is retarded when the EphA2 to ALCAM (E/A) ratio falls below a threshold.

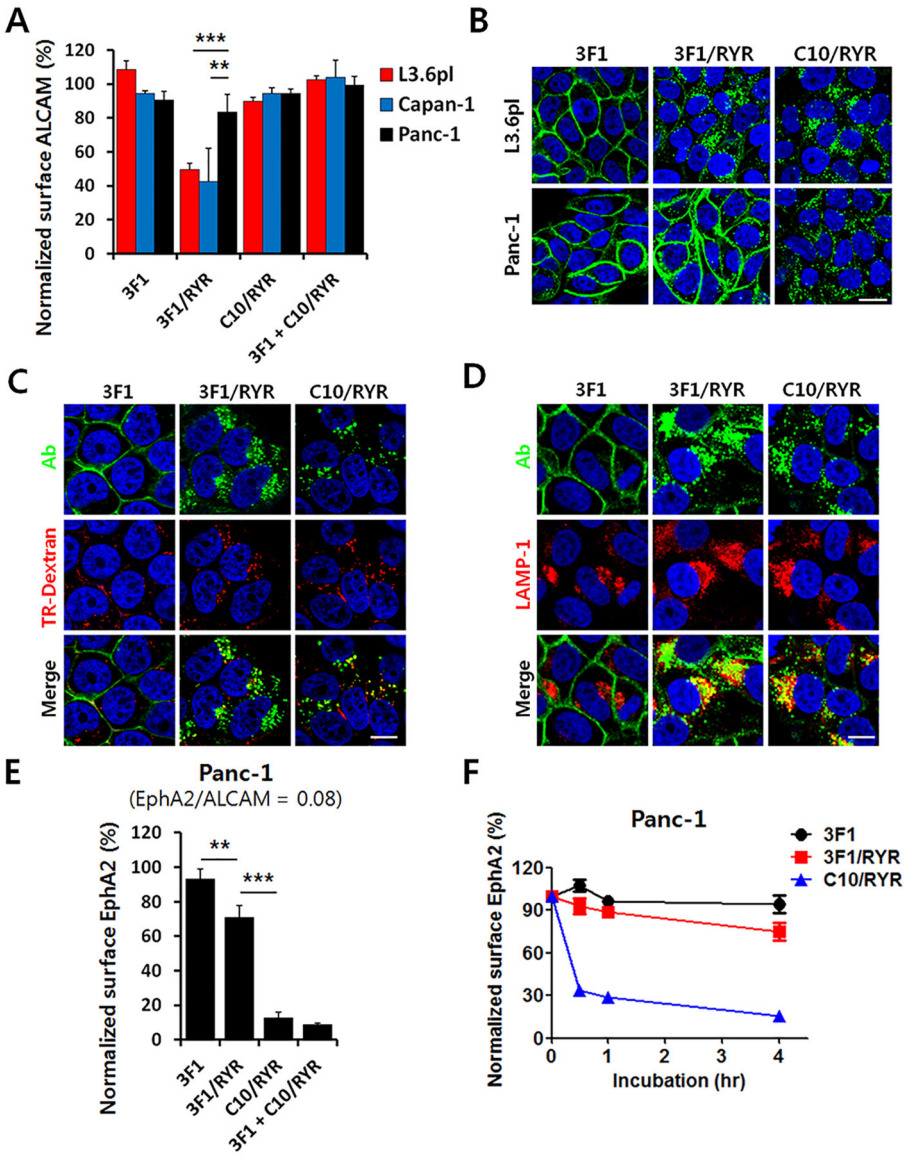

Fig. 2. The bispecific 3F1/RYR effectively removes the non-internalizing antigen ALCAM from pancreatic cancer cell surface.

A) ALCAM cell surface level post antibody treatment. Pancreatic cancer cell lines (L3.6pl, Capan-1, Panc-1) were incubated with 3F1, 3F1/RYR, C10/RYR, or a mixture of 3F1 and C10/RYR. Following wash post treatment, cell surface ALCAM level was determined using an Alexa® 647-labeled IgG that bind to a different epitope on ALCAM than 3F1. MFI values were normalized against cells without antibody treatment. **P<0.01, and ***P<0.001. Duplicates. B) Confocal microscopy study of cell-type selective internalization mediated by the bispecific. L3.6pl (E/A ratio > 0.2) and Panc-1 (E/A ratio < 0.2) cells were incubated with 3F1, 3F1/RYR, or C10/RYR, and internalizing antibodies were stained with FITC-labeled anti-human IgG. Scale bar: 20 μm. C) Co-localization of antibodies and macropinocytotic vesicles. L3.6pl cells were incubated with 3F1, 3F1/RYR, or C10/RYR at 100 nM and ND70-TR (TR-Dextran, *red*) for 2 hours. Antibodies were detected by FITC-labeled anti-human IgG (*green*). Nuclei were labeled with Hoechst 33342 (*blue*). Scale bar:

10 μm. D) Lysosomal trafficking post internalization. L3.6pl cells were incubated with indicated antibodies (100 nM) for 2 hours. Internalized antibodies (*green*) and nuclei (*blue*) were stained as described in C), and lysosomes were detected using rabbit anti-LAMP1 primary IgG, followed by Alexa® 647-labeled anti-rabbit IgG (*red*). Scale bar: 10 μm. E) Retarded EphA2 internalization on Panc-1 cell when targeted by the bispecific. **P<0.01, and ***P<0.001. Duplicates. F) A time course of EphA2 removal from Panc-1 cell surface at 0.5, 1, and 4 hours post antibody treatment.

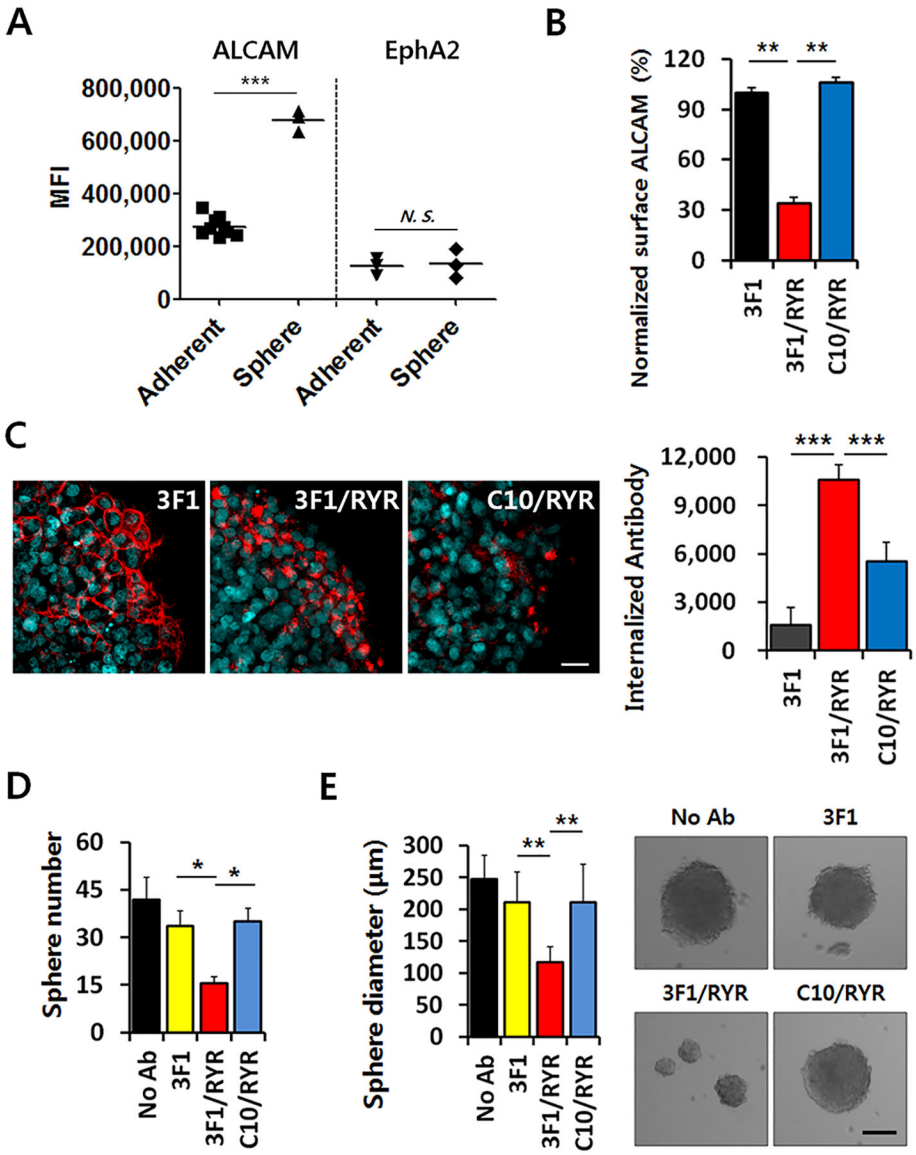

Fig. 3. Bispecific-induced cell surface ALCAM removal has an anti-clonogenic effect on pancreatic tumor-spheres.

A) Significant ALCAM upregulation on L3.6pl sphere cells compared to non-sphere tumor cells. Adherent- or sphere-cultured L3.6pl cells were separated into single cells and antigen expression was measured using 3F1 or RYR IgG, followed by Alexa® 647-labeled anti-human IgG. The EphA2/ALCAM ratio is ~ 0.15 for sphere and ~ 0.305 for monolayer cells. B) ALCAM removal from the surface of sphere-forming cells by 3F1/RYR. Single cell population of L3.6pl (200 cells/well) was incubated with indicated antibodies (100 nM) for 2 weeks in an ultra-low attachment well plate. Cell surface levels of ALCAM post antibody treatment were determined by FACS. MFI values were normalized against control (no antibody treatment). **P<0.01. Duplicates. C) Antibody internalization into L3.6pl spheres. Tumor spheres incubated with indicated antibodies were collected by centrifugation, fixed, and permeabilized for confocal microscopy analysis. Antibodies and nuclei were stained with Alexa® 647-labeled anti-human IgG (*red*) and Hoechst 33342 (*cyan*), respectively.

Scale bar: 10 μm. Intracellular antibody fluorescence intensity was quantified by Image J and shown in the right panel. ***P<0.001. D) Inhibition of L3.6pl tumor sphere formation by 3F1/RYR – reduction in number. Tumor sphere numbers (> 100 μm) were counted 14 days post antibody treatment (left) with representative well images shown (right). Error bars represent SD of a duplicate. *P < 0.05. E) Inhibition of L3.6pl tumor sphere formation by 3F1/RYR – reduction in size. **P<0.01. Duplicates. Scale bar: 100 μm.

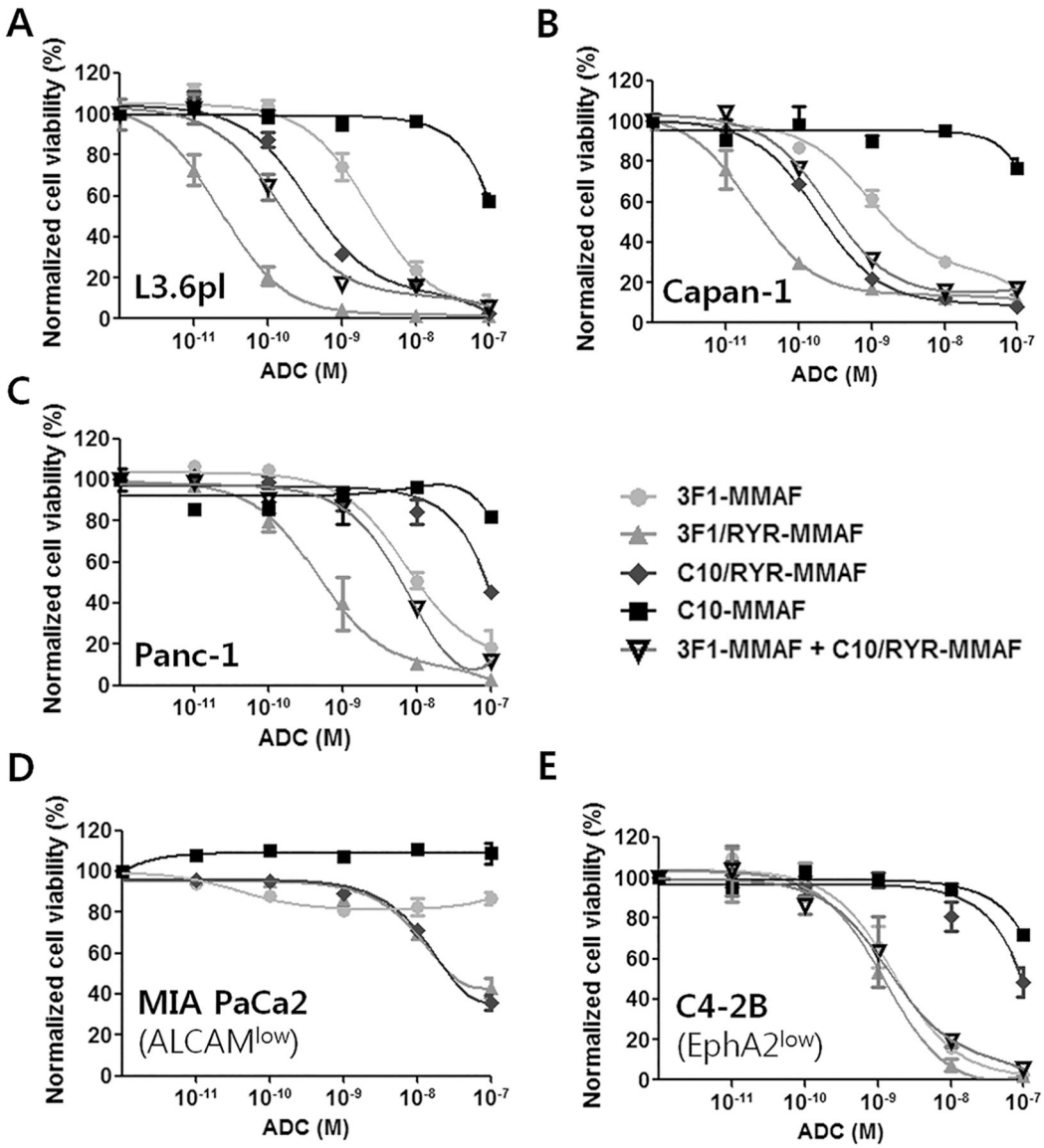

Fig. 4. ***In vitro*** **potency and selectivity of ADCs with site-specific conjugation on tumor cell lines with varying EphA2/ALCAM ratios.**

Cytotoxicity of indicated ADCs or a mixture was studied on L3.6pl (A) and Capan-1 (B) cell lines with relatively high EphA2/ALCAM ratios, and Panc-1 (C) cell line that has a low EphA2/ALCAM ratio. MIA PaCa2 (D) and C4–2B (E) cell lines were utilized as an ALCAM-low/negative and EphA2-low/negative cancer cell model, respectively. Cell viability (%) was normalized against a control group without ADC treatment.

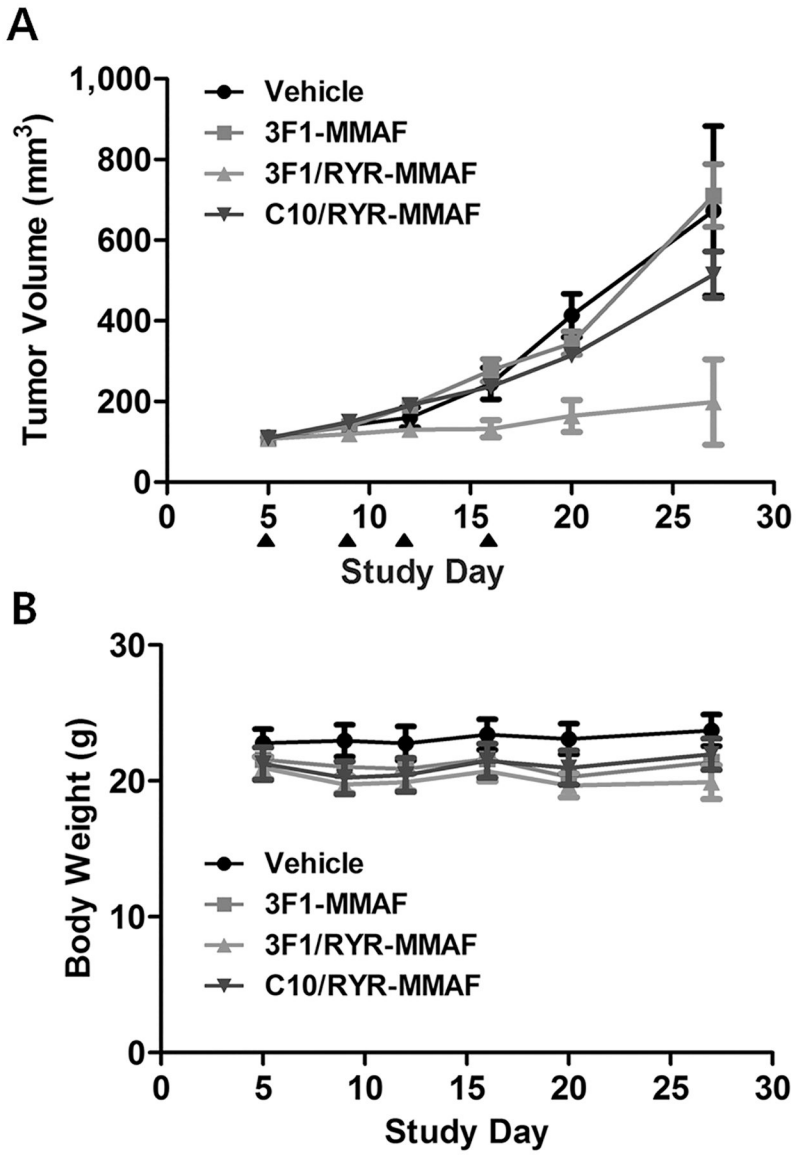

Fig. 5. Anti-tumor efficacy of the bispecific 3F1/RYR ADC in a pancreatic cancer xenograft model.

A) Effect on tumor growth. Mice were inoculated subcutaneously with 1×10^6 Capan-1 cells and randomly divided into 4 groups (6 mice/group) with similar average tumor size. Vehicle (PBS) or ADCs (3 mg/kg) were intravenously injected at indicated time points (*arrow head*). The mean tumor volumes ± SEM (mm^3) was plotted. B) Body weight was monitored and plotted to assess toxicity of ADC treatment. No significant body weight loss (e.g., > 15%) was seen for any of the groups studied.

Table 1.

Summary of antigen density, guide to effector ratio, and ALCAM turnover efficiency on various cell line models.

Cell models		Antigen density and ratio (Mean±SD, n=2)			ALCAM Intern over ctrl, Me	
		EphA2	ALCAM	EphA2/ALCAM	3F1	3F1/RYI
HEK293		5,064 ± 858	335,719 ± 2,475	0.02	6.6	19.6
Transiently EphA2-transfected HEK293	HEK293-EphA2–0.02	357,994 ± 83,557	286,531 ± 6,581	1.25	29.4	68.9
	HEK293-EphA2–0.1	1,081,566 ± 89,489	325,339 ± 17,985	3.32	7.7	68.9
	HEK293-EphA2–0.5	2,130,189 ± 210,485	311,259 ± 42,142	6.84	3.5	70.1
	HEK293-EphA2–2.5	3,386,996 ± 236,937	301,854 ± 3,913	11.22	21.3	71.2
Stably EphA2-expressing HEK293	HEK293-EphA2#C9	18,398 ± 1,606	320,850 ± 36,242	0.06	2.8	20.7
	HEK293-EphA2#42	23,508 ± 2,955	202,617 ± 11,141	0.12	3.7	16.5
	HEK293-EphA2#8	1,876,422 ± 224,373	279,389 ± 11,756	6.72	−17.9	87.2
	HEK293-EphA2#2	2,864,233 ± 409,871	295,696 ± 9,053	9.69	−7.8	89.1
	HEK293-EphA2#31	4,608,433 ± 50,555	278,564 ± 2,880	16.54	−11.7	87.6
Transiently ALCAM-siRNA/EphA2-transfected HEK293	HEK293-siRNA1	466,203 ± 82,224	296,677 ± 63,749	1.57	−7.5	70.2
	HEK293-siRNA2	377,816 ± 95,592	208,304 ± 23,759	1.81	−14.0	69.7
	HEK293-siRNA3	507,760 ± 17,793	60,512 ± 5,047	8.39	−6.6	87.5